Communications In Catalysis
Vol. 1, No. 2, 2024, pp.35-56
DOI: 10.22049/CIC.2018.26341.1022

Azarbaijan Shahid Madani University

Tetracycline and Doxycycline photocatalytic degradation by Nano α-Fe_2O_3/12-tungstosilicic acid prepared through forced hydrolysis and reflux condensation

Majid Saghi, Kazem Mahanpoor*

Department of Chemistry, Arak Branch, Islamic Azad University, Arak, Iran , P.O. Box 38135/567,.

* Corresponding Author. Tel: +988633412222.

E-mail: address: k-mahanpoor@iau-arak.ac.ir

Received: 2024-11-20, Revised: 2024-12-03, Accepted: 2024-12-12

Abstract

In the research, spherical α-Fe_2O_3 nanoparticles (NPs) were synthesized and supported on the surface of 12-tungstosilicic acid (12-TSA.7H_2O) using forced hydrolysis and reflux condensation (FHRC) method. Photocatalytic activity of pure and supported α-Fe_2O_3 NPs (α-Fe_2O_3/2-TSA.7H_2O) for Tetracycline (TC) and Doxycycline (DC) degradation was investigated using UV/H_2O_2 process. The products were characterized by FTIR, SEM/EDX, BET surface area and XRD. The experiments were designed considering four variables including pH, the initial concentration of pollutant, catalyst concentration and H_2O_2 concentration at two-levels and three central point's using full factorial experimental design. The results indicated that supporting α-Fe_2O_3 NPs caused to improve the filtration, recovery and photocatalytic activity of NPs. Under optimal conditions, 88.44% TC and 87.67% DC were degraded following 50 and 120 min, respectively. The results indicated that reactions follows first-order kinetic and rate coefficient for TC and DC degradation reactions equals to 0.0178 and 0.0074 min^{-1}, respectively.

Keywords: Tetracycline; Doxycycline; Full factorial; α-Fe_2O_3; α-Keggin.

Introduction

The numerous reports have stated the existence of antibiotics such as TC and DC in water resources such as urban and industrial wastewaters, drinking waters, surface waters and ground waters [1-6]. It is common to use photocatalytic processes for degradation of pharmaceutical pollutants but using effective, economically-reasonable and recoverable catalysts is highly important. In some photocatalytic processes, it is necessary to use supported catalysts. The supported catalysts comprise two major segments: catalyst and catalyst support. Catalyst is commonly made up of active and effective segment of these composites but there are numerous cases where catalyst support is active too [7]. Using the supported catalysts could be due to different causes but enhancing the catalytic activity and their more convenient recovery are two common purposes for affixing catalyst on the surface of catalyst support. Various organic, inorganic or organic/inorganic materials could be used as catalyst support [8, 9]. Selecting the suitable catalyst support depends to some factors such as conditions governing the process, chemical and physical properties of the desirable catalyst and catalyst support, etc. Polyoxometalates (POMs) are a class of inorganic compounds as multi-core clusters which could be used as catalyst support [10]. POMs are divided into two categories of isopolyanions (IPAs) and heteropolyanions (HPAs). In molecular structure of IPAs, there are only oxygen and metal atoms, whereas HPAs have at least one hetero atom (Si, P, As, B, etc.) in addition to metal and oxygen [11]. Thermodynamically, HPAs have stable arrangements and maintain their crystal structure in aqueous and non-aqueous solutions; therefore they could be used as catalyst support under different conditions. This class of materials has various applications in catalysis [12], analytical chemistry [13], medicinal chemistry (anti-tumor, anti-cancer, anti-bacteria, anti-microbial and anti-clotting) [14-16], radioactive materials [17] and gas absorbents [18]. HPAs have different structures of which α-, β-, γ-, δ- and ε-Keggin, Wells–Dawson, Preysler, Strandberg and Anderson–Evans are served as critical types. 12-TSA is a HPA with formula $H_4SiW_{12}O_{40}$ and α-Keggin structure (see Figure 1). The central Si heteroatom is surrounded by a tetrahedron whose oxygen vertices are each linked to one of the four W_3O_{13} sets. Each W_3O_{13} consists of three W_3O_6 octahedrals linked in a triangular arrangement by sharing edges and the four W_3O_{13} are linked together by sharing corners [19].

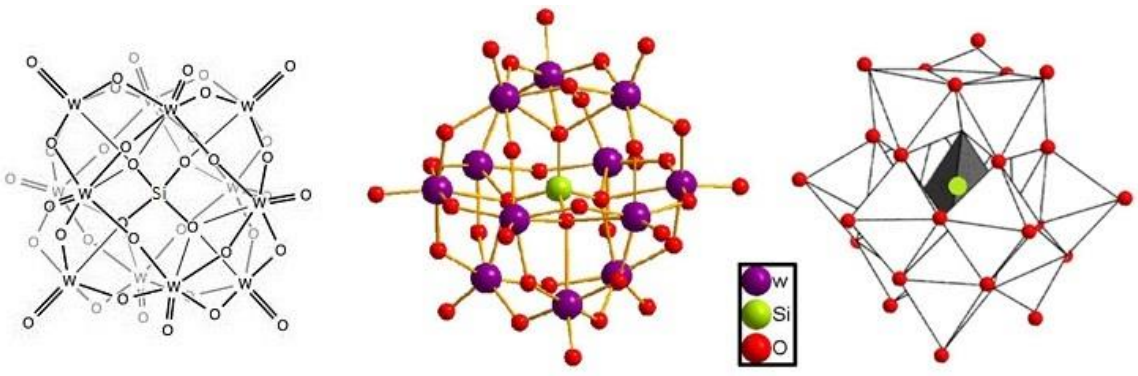

Figure. 1 α-Keggin structure of $[SiW_{12}O_{40}]^{4-}$.

Using nanocatalysts (Those catalysts whose particles are 1-100 nm) could be more effective in photocatalytic processes. Metal oxide NPs i.e., iron oxides, have a special position in the science and technologies because of having wide applications and unique properties [20-22]. α-Fe_2O_3 (hematite) which is the most common form of iron oxides, has the rhombohedral structure and it is an attractive compound because of its applications in data storage, gas sensor, magnets materials, pigment, catalysis and photocatalysis [23-28]. Various techniques including co-precipitation, sol-gel, thermal decomposition, Micelle synthesis, sonochemical synthesis, hydrothermal synthesis and FHRC have been utilized to synthesize monodisperse α-Fe_2O_3 NPs [29-35]. Since chemical degradation and removing the pollutants existed in aqueous medium is one of most critical use of photocatalytic processes, so using supported catalysts could be very helpful because in addition to increase the performance of degradation, it provides convenient recovery of catalyst from polluted solution and its reuse. In order to optimize a process like the photocatalytic degradation process, it is essential to study all factors influencing the process. But studying the effects of individual factors on the process is difficult and time-consuming, especially if these factors are not independent and they affect each other. Employing experimental design could eliminate these problems because the interaction effects of different factors could be attained using design of experiments (DoEs) only. Full factorial is an appropriate method for DoEs because it could reduce the total number of experiments as well as optimize the process by optimizing all the affecting factors collectively, at a time [36]. The design could determine the effect of each factor on the response as well as how this effect varies with the change in level of other factors. In the paper, spherical α-Fe_2O_3 nanoparticles were synthesized and supported on the surface of 12-TSA using FHRC method. The catalyst of α-Fe_2O_3/12-TSA was used in order to remove TC and DC antibiotics under UV/H_2O_2 process. The molecular structures of TC and DC are shown in Figure 2.

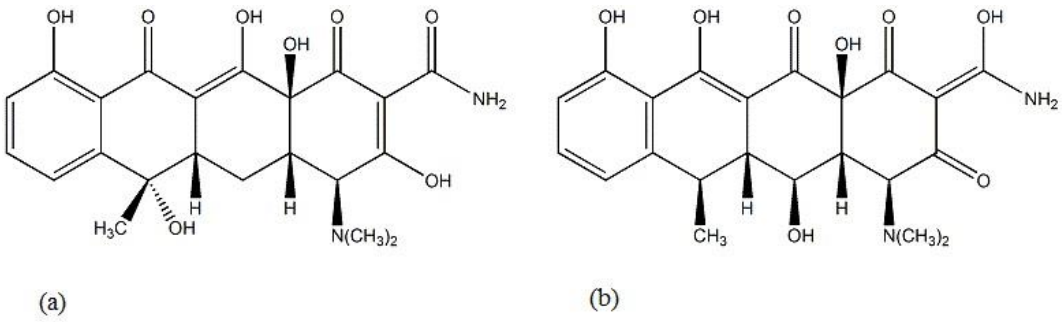

Figure 2. TC (a) and DC (b) Molecular structures.

Experimental

Material and Apparatuses

All chemicals including sodium tungstate dihydrate, sodium silicate, diethyl ether, iron (III) chloride hexahydrate, urea, hydrogen peroxide (30%), hydrochloric acid (37%), sulfuric acid (96%), sodium hydroxide and ethanol were purchased from Merck. Also, the required TC and DC were purchased from Razak and Iran Daru pharmaceutical laboratories, respectively. Deionized water was used throughout the experiments. The Fourier Transform Infra-Red (FTIR) spectra of products were recorded on a Perkin-Elmer spectrophotometer (Spectrum Two, model) in the range of 450-4000 cm^{-1}. The shape, morphology and elemental analysis of 12-TSA.7H_2O and α-Fe_2O_3/12-TSA.7H_2O surfaces were examined using a Philips XL-30 Scanning Electron Microscope/Energy Dispersive X-ray spectroscopy (SEM/EDX). The X-Ray Diffraction (XRD) analysis of the samples was done using a DX27-mini diffractometer and BET surface area of materials was determined by N_2 adsorption–desorption method at 77 K, measured using a BELSORP-mini II instrument. Also, all Ultraviolet/Visible (UV/Vis) absorption spectra were obtained using an Agilent 8453 spectrophotometer.

Synthesis of α-Fe_2O_3 NPs

The synthesis of α-Fe_2O_3 NPs was carried out according to Bharathi et al [35]. Firstly, 100 ml iron (III) chloride hexahydrate 0.25 M was poured into a flat-bottom flask. When iron solution was agitated, it was added drop by drop to it 100 ml urea 1 M. The obtained mixture was stirred for 30 min and then placed under the reflex at 90-95 ^oC for 12 h. Then, the precipitate after separation was washed with 100 ml deionized water because unreacted ions will be completely removed. The washed precipitate was dried at 70 ^oC for 2 h. Finally, this solid remained at 300 ℃ for 1 h, hence the iron hydroxide particles will transform to iron oxide.

Synthesis of 12-TSA.7H_2O

12-TSA.7H_2O was synthesized according to literature procedure [37]. Firstly, 15 g sodium tungstate dihydrate was dissolved in 30 ml deionized water and then 1.16 g sodium silicate solution with a density of 1.375 g/ml was added to it. The resulted mixture was heated up to about boiling point, and while it was stirred, 10 ml concentrated HCl was added to it during 30 min, smoothly. Then, the solution was naturally cooled down to room temperature and slight precipitate formed (silicic acid) in it was filtered. Again, 5 ml concentrated HCl was added to the solution and was transferred to separatory funnel after cooling it again down to room temperature. Then, 12 ml diethyl ether was added to it and well shaken. Therefore, three layers were formed inside separatory funnel, middle layer of which was yellow-colored. Bottom layer which was oily ether was separated and transferred into a beaker. In order to further extract, separatory funnel was further shaken again and the bottom layer was once more separated and transferred into the beaker. The extraction process was done so much that the yellow color of middle layer was fully faded. The extracted ether complex

which was inside the beaker was transferred to another separatory funnel and then 16 ml HCl 25% v/v was added to it. Next, 4 ml diethyl ether was added to it, subsequently. The contents inside separatory funnel were shaken and bottom layer (ether) was transferred to the evaporating dish after separating. Evaporating dish was exposed to air and remained motionless to evaporate the solvent and form the 12-TSA.7H_2O crystals. Finally, 12-TSA.7H_2O formed crystals were placed at 70 ^oC for 2 h until it was completely dried. The chemical reaction occurred in the process of 12-TSA.7H_2O synthesis has been shown in (1) [37].

(1) $12\ Na_2WO_4 + Na_2SiO_3 + 26\ HCl \rightarrow H_4SiW_{12}O_{40}.xH_2O + 26\ NaCl + 11\ H_2O$

Preparation of α-Fe_2O_3/12-TSA.7H_2O (FHRC method)

Firstly, 50 ml iron (III) chloride hexahydrate 0.25 M was poured into a beaker. While it was agitated by stirrer, 3.5 g 12-TSA.7H_2O was gently added to it. The obtained mixture was stirred for 4-5 h. The solid accumulated at bottom of beaker was separated and transferred into one flat-bottom flask and the same 10 ml solution inside beaker was added to it. When mixture was being stirred, 50 ml urea 1 M was gradually added to it. The mixture was placed under reflux at 90-95 ^oC for 12 h. Then, the precipitate resulted after separation was washed with 100 ml ethanol/deionized water 1:1 solution because unreacted ions were completely removed. The washed precipitate was dried at 80 ^oC for 2 h. In order to calcination, the obtained solid was kept at 300 ^oC for 1 h.

Experimental design

The photocatalytic efficiency of products on the TC and DC degradation was investigated using full factorial experimental design. The experiments were designed considering four variables including pH, the initial concentration of pollutant, catalyst concentration and H_2O_2 concentration at two-levels and three central points. Experimental range and levels of variables are shown in Table 1. Also, 19 experiments related to this factorial have been listed in Table 2.

Table 1. Experimental range and levels of the variables

Variables	Range and levels					
	For TC pollutant			For DC pollutant		
	–1	0	+1	–1	0	+1
pH	4	6	8	4	6	8
Initial Con. of pollutant (ppm)	30	50	70	80	100	120
Catalyst Con. (ppm)	50	100	150	100	125	150
H_2O_2 Con. (ppm)	0.1	0.3	0.5	1	1.5	2

Table 2. Experimental conditions for photocatalytic process

Exp. No.	Variable			
	pH	Initial Con. of pollutant (ppm)	Catalyst Con. (ppm)	H_2O_2 Con. (ppm)
1	–1	–1	–1	–1
2	+1	–1	+1	+1
3	–1	–1	+1	–1
4	–1	+1	+1	–1
5	+1	+1	+1	–1
6	0	0	0	0
7	+1	–1	+1	–1
8	–1	+1	–1	+1
9	+1	–1	–1	–1
10	+1	+1	+1	+1
11	–1	+1	–1	–1
12	+1	–1	–1	+1
13	+1	+1	–1	–1
14	–1	+1	+1	+1
15	+1	+1	–1	+1
16	0	0	0	0
17	–1	–1	+1	+1
18	0	0	0	0
19	–1	–1	–1	+1

General procedure

Figure 3 shows one schematic diagram of photocatalytic reactor used in the work. An MDF box was designed inside which a circular Pyrex reactor was placed. On the upper section of the box, three mercury lamps were built-in as UV light sources. The radiation is generated almost exclusively at 254 nm. The liquid inside the reactor was agitated by magnetic stirrer and the air inside the box was conditioned by a fan. In order to carry out each experiment, firstly 250 ml polluted solution was made as specified concentration and poured inside the reactor. Then, at related pH, the specified amount of catalyst and H_2O_2 were added to the solution inside the reactor. In all experiments, pH adjustment was done via minimum use of H_2SO_4 and NaOH. Then, stirrer and UV lamps were immediately turned on to initiate the process. In order to fully separate the catalyst from solution, the samples were centrifuged for 3 min with 3500 rpm speed. The concentrations of TC and DC in the samples were determined using a UV/Vis spectrophotometer at λ_{max}=357 and 347 nm, respectively. The percentage of pollutant decomposition (x%) as a function of time is given by

$$x\% = \frac{C_0 - C}{C_0} \times 100 \quad (2)$$

Where C_0 and C are the concentration of pollutant (ppm) at t=0 and t, respectively.

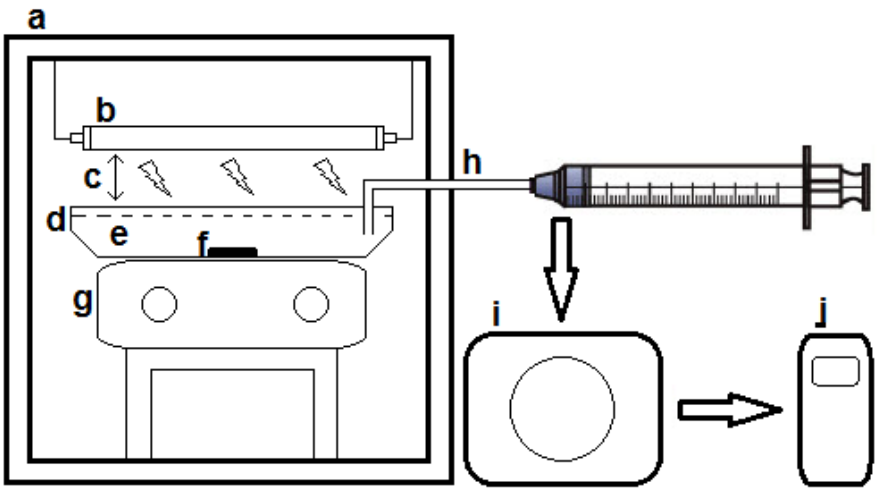

Figure 3. Schematic diagram of photo reactor.
(a) MDF box, 50×50×50 cm; (b) Mercury lamps, Philips 15W; (c) The distance between surface of polluted solution and lamps, 5 cm; (d) Reactor, 300 ml capacity; (e) The polluted solution, 250 ml; (f) Magnet; (g) Magnetic stirrer; (h) Sampling port; (i) Centrifuge, 3 min; (j) UV/Vis spectrophotometer.

Result and Discussions

Characterization of 12-TSA.7H$_2$O

SEM image of 12-TSA.7H$_2$O is shown in Figure 4. Suitable area and the pores existed on the surface of this catalyst support provide an appropriate conditions to support α-Fe$_2$O$_3$ NPs. IR is a suitable method for the structural characterization of HPAs [11]. FTIR spectrum of the synthesized 12-TSA.7H$_2$O has been shown in Figure 5a. There are four kinds of oxygen atoms in 12-TSA.7H$_2$O structure, 4 Si-O$_a$ in which one oxygen atom connects to Si, 12 W-O$_b$-W oxygen bridges (corner-sharing oxygen-bridge between different W$_3$O$_{13}$ groups), 12 W-O$_c$-W oxygen bridges (edge-sharing oxygen-bridge within W$_3$O$_{13}$ groups) and 12 W=O$_d$ terminal oxygen atoms. The symmetric and asymmetric stretching of the different kinds of W-O bonds are observed in the following spectral regions: Si-O$_a$ bonds (1020 cm^{-1}), W=O$_d$ bonds (1000-960 cm^{-1}), W-O$_b$-W bridges (890-850 cm^{-1}), W-O$_c$-W bridges (800-760 cm^{-1}) [38]. In Table 3, vibrational frequencies of the synthesized 12-TSA.7H$_2$O and equivalent values reported in previous studies [38, 39] have been listed. Comparing the vibrational frequencies reveals that 12-TSA.7H$_2$O has been well synthesized. XRD is one of the most important characterization tools used in solid state chemistry and materials science. Figure 6a shows the XRD pattern of 12-TSA.7H$_2$O. This pattern indicates that the characteristic peaks corresponded to the 12-TSA were well appeared and it means that the synthesized 12-TSA.7H$_2$O crystals were well formed [39].

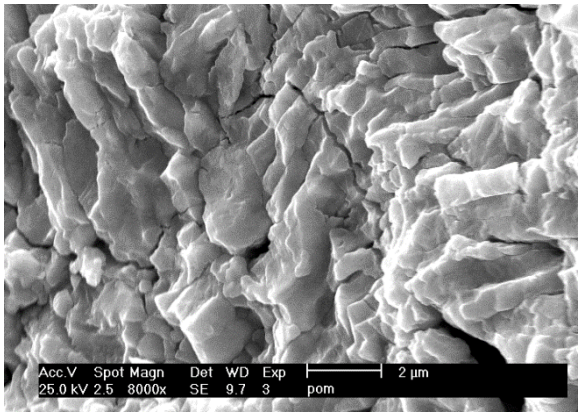

Figure 4. SEM image of the synthesized 12-TSA.7H_2O.

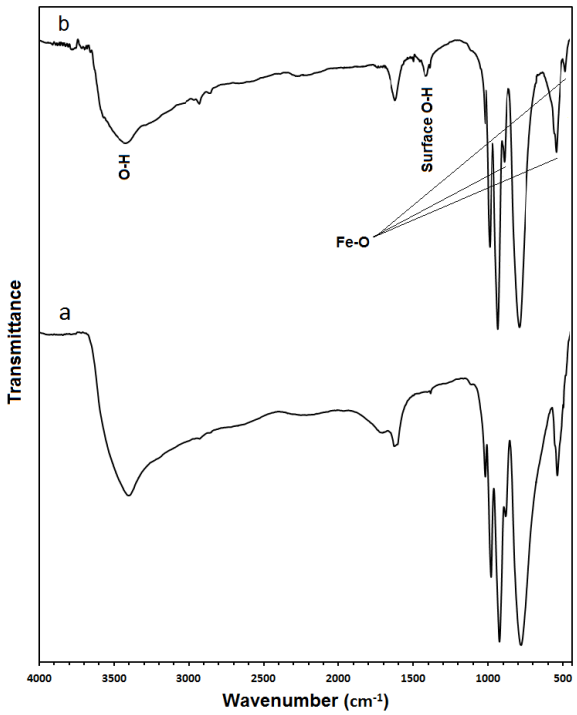

Figure 5. FTIR spectra of the synthesized 12-TSA.7H_2O (a) and α-Fe_2O_3/12-TSA.7H_2O (b).

Table 3. Vibrational frequencies of the synthesized 12-TSA.7H_2O and equivalent values reported in previous reports

Number	The synthesized 12-TSA.7H_2O		[38, 39]
	Wavenumber (cm^{-1})	Transmittance %	
1	1019.04	13.29	1020 (weak)
2	980.68	8.81	981 (sharp)
3	924.31	5.92	928 (very sharp)
4	882.63	11.52	880 (medium)
5	780.28	5.77	785 (very sharp)
6	537.41	13.35	540 (medium)

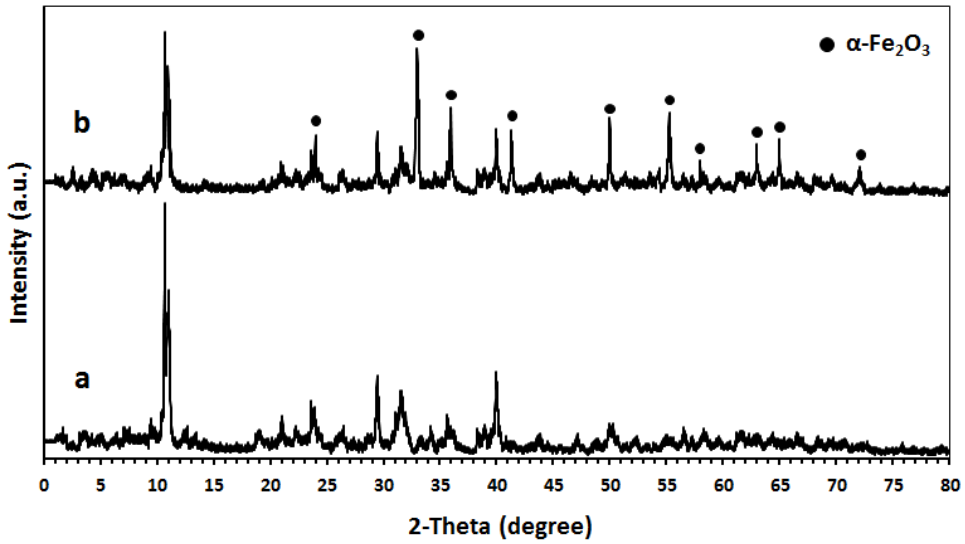

Figure 6. X-ray diffractogram of the synthesized 12-TSA.7H_2O (a) and α-Fe_2O_3/12-TSA.7H_2O (b).

Characterization of α-Fe_2O_3/12-TSA.7H_2O

Figure 7 shows SEM/EDX results of α-Fe_2O_3/12-TSA.7H_2O. SEM image indicate that α-Fe_2O_3 particles were spherically supported on the surface of 12-TSA.7H_2O. In the EDX spectrum, peaks of three main elements in α-Fe_2O_3/12-TSA.7H_2O namely Si, W and Fe were appeared and named. Au peaks in the EDX spectrum is due to samples coverage's with a thin layer of gold before SEM/EDX analysis. Generally, the result of EDX indicated that α-Fe_2O_3 particles were supported on the surface of 12-TSA.7H_2O. In Figure 5b, FTIR spectra of α-Fe_2O_3/12-TSA.7H_2O have been shown. It is clear that absorption peaks of 12-TSA.7H_2O have appeared without considerable change in the wavenumbers (only their intensities have been slightly changed). It means that 12-TSA.7H_2O was stable and it had not been changed chemically during preparing α-Fe_2O_3/12-TSA.7H_2O. Also, absorption peaks of α-Fe_2O_3 have well appeared and are in agreement with results of Bharathi et al [35]. These absorption peaks which are related to stretching and bending modes of OH and Fe-O binding in FeOOH, in some cases overlapped with absorption peaks of 12-TSA.7H_2O. In Fig. 6b, XRD pattern of α-Fe_2O_3/12-TSA.7H_2O have been illustrated. In the pattern, characteristic peaks of 12-TSA.7H_2O have well appeared which indicates that 12-TSA.7H_2O was stable during the supporting process. Also, characteristic peaks of α-Fe_2O_3 which have also been marked have appeared and it is in agreement with results of Bharathi et al [35]. The size of spherical α-Fe_2O_3 particles supported on the surface of 12-TSA.7H_2O were calculated using XRD and Warren-Averbach method (taking account of device errors) [40] whose averages were 70.82 nm. The BET surface area of α-Fe_2O_3/12-TSA.7H_2O was determined 39.84 (m^2/g).

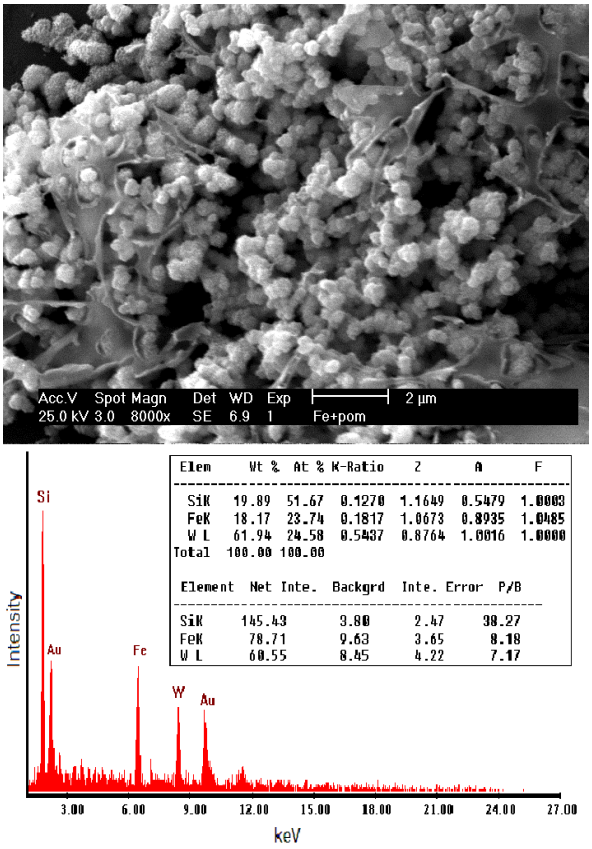

Figure 7. SEM image (top) and EDX re (bottom) of α-Fe_2O_3/12-TSA.7H_2O.

UV/Vis spectra

The absorbance of TC solutions during photocatalytic process (according to Exp. No. 15) at initial and after 10, 20, 30, 40 and 50 min irradiation time verses wavelength are depicted in Figure 8. Also, the absorbance of DC solutions (based on Exp. No. 11) at initial and after 20, 40, 60, 80, 100 and 120 min irradiation time has been shown in Figure 9.

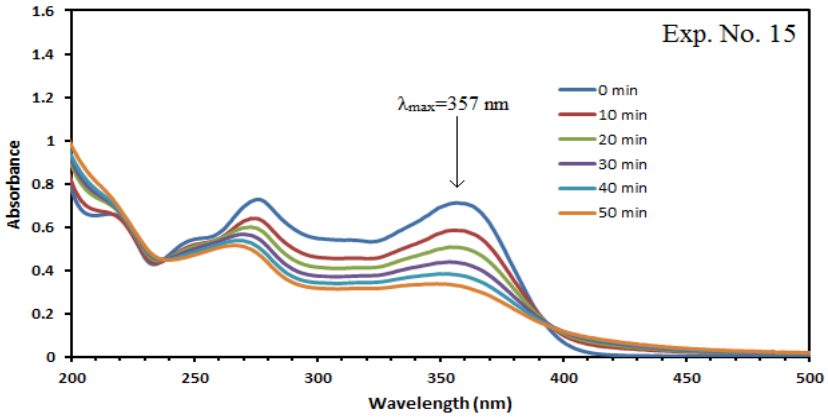

Figure 8. UV/Vis spectral absorption changes of TC solution photodegraded by α-Fe_2O_3/12-TSA.7H_2O (pH=8, Initial concentration of TC=70 ppm, catalyst concentration=50 ppm, H_2O_2 concentration=0.5 ppm).

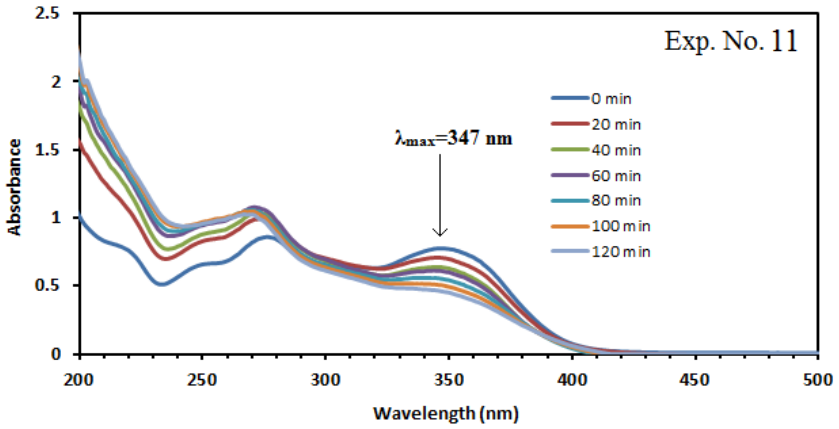

Figure 9. UV/Vis spectral absorption changes of DC solution photodegraded by α-Fe_2O_3/12-TSA.7H_2O (pH=4, Initial concentration of DC=120 ppm, catalyst concentration=100 ppm, H_2O_2 concentration=1 ppm).

Performance of photocatalysts

Having carried out all experiments based on Table 1, x% values were calculated which have been reported in Table 4. In general, comparing x% values reveal that the degree of pollutants photocatalytic degradation by pure α-Fe_2O_3 is lower than that of α-Fe_2O_3/12-TSA.7H_2O. This means that supporting α-Fe_2O_3 NPs leads to increase their photocatalytic activity. Also, the results show that in the best manner, 88.44 % TC and 87.67 % DC were degraded using α-Fe_2O_3/12-TSA.7H_2O.

Table 4. x% values

Exp. No.	x%			
	α-Fe_2O_3		α-Fe_2O_3/12-TSA.7H_2O	
	TC	DC	TC	DC
1	64.11	62.24	66.32	78.19
2	75.39	60.33	85.95	74.65
3	67.56	75.27	73.29	84.62
4	48.83	51.16	53.22	72.66
5	37.14	36.62	45.07	64.93
6	36.97	54.37	60.38	74.08
7	82.17	55.72	88.44*	83.09
8	37.95	38.4	43.64	66.15
9	65.46	60.78	74.61	72.99
10	44.37	53.32	47.92	73.67
11	32.84	36.59	38.91	65.17
12	62.00	60.83	74.28	74.66
13	29.84	44.43	37.71	69.22
14	40.69	65.77	48.72	80.09
15	39.31	52.81	45.62	73.09
16	37.02	54.45	59.79	74.44
17	66.83	81.15	77.13	87.67*
18	36.83	53.97	60.13	73.78
19	65.83	52.43	80.86	73.28

* Maximum value of x%

Photocatalytic mechanism

According to Exp. Nos. 7 and 17, the effects of UV irradiation, H_2O_2, pure α-Fe_2O_3 NPs and α-Fe_2O_3/12-TSA.$7H_2O$ on the degradation of TC and DC are presented in Figures 10 and 11, respectively. Figure 10 designate that in the presence of α-Fe_2O_3/12-TSA.$7H_2O$, H_2O_2 and UV irradiation 88.44% of TC was degraded at the reaction time of 50 min while it was 82.17% and 10.2% for pure α-Fe_2O_3 NPs and only UV, respectively. These values for DC following 120 min reaction were 87.67, 81.15 and 8.7, respectively (see Figure 11).

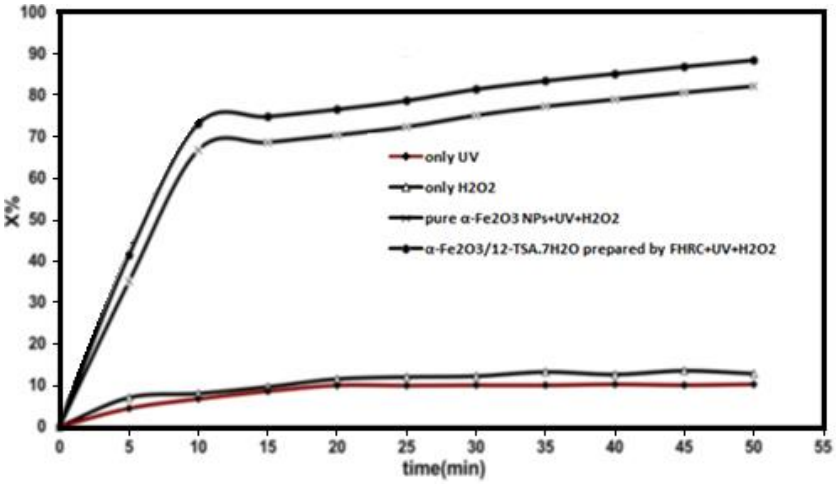

Figure 10. Effect of UV light, H_2O_2, α-Fe_2O_3 and α-Fe_2O_3/12-TSA.$7H_2O$ on TC degradation.

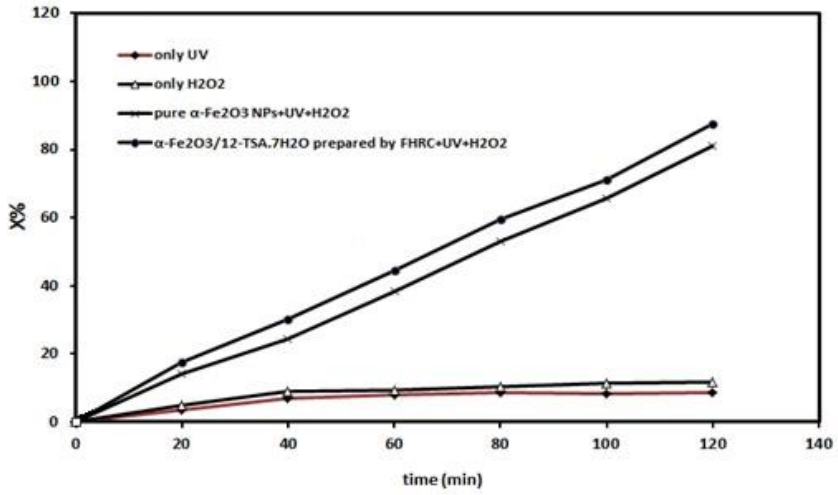

Figure 11. Effect of UV light, H_2O_2, α-Fe_2O_3 and α-Fe_2O_3/12-TSA.$7H_2O$ on DC degradation.

When α-Fe_2O_3 is illuminated by the light, electrons are promoted from the valence band (VB) to the conduction band (CB) of the semi conducting oxide to give electron-hole pairs. The VB potential (h_{VB}) is positive enough to generate hydroxyl radicals at the surface, and the CB potential (e_{CB}) is negative enough to reduce

molecular oxygen. The hydroxyl radical is a powerful oxidizing agent and attacks TC or DC molecules present at or near the surface of α-Fe_2O_3. It causes the photo-oxidation of TC or DC according to the following reactions [41, 42]:

(3) α-Fe_2O_3 + *hν* → α-Fe_2O_3 (e^-_{CB} + h^+_{VB})
(4) h^+_{VB} + $H_2O_{(ads)}$ → H^+ + $^{\bullet}OH^-_{(ads)}$
(5) h^+_{VB} + $OH^-_{(ads)}$ → $^{\bullet}OH_{(ads)}$
(6) e^-_{CB} + $O_{2(ads)}$ → $^{\bullet}O^-_{2(ads)}$
(7) H_2O □ $H^+ + OH^-$
(8) $^{\bullet}O^-_{2(ads)}$ + H^+ → $^{\bullet}HO_2$
(9) $2\,^{\bullet}HO_2$ → H_2O_2 + O_2
(10) H_2O_2 + α-Fe_2O_3 (e^-_{CB}) → $^{\bullet}OH$ + OH^- + α-Fe_2O_3
(11) $^{\bullet}OH_{(ads)}$ + TC or DC → Degradation of TC or DC
(12) h^+_{VB} + TC or DC → $TC^{\bullet+}$ or $DC^{\bullet+}$ → Oxidation of TC or DC

The above mechanism is summarized in Figure 12. The main role of the catalyst support is creating the perfect conditions for putting the TC or DC and hydroxyl radical beside each other. Photocatalytic activity increased after stabilizing iron oxide on 12-TSA.7H_2O. To comment on this result, we propose that the hydroxyl radicals, on the surface of iron oxide, are easily transferred onto the surface of 12-TSA.7H_2O. That means the organic pollutants such as TC and DC, which have already been adsorbed on the nonphotoactive α-Fe_2O_3/12-TSA.7H_2O, have chances to be degraded due to the appearance of hydroxyl radicals, resulting in the enhancement of the photodegradation performance of α-Fe_2O_3/12-TSA.7H_2O (as shown in Figure 12b).

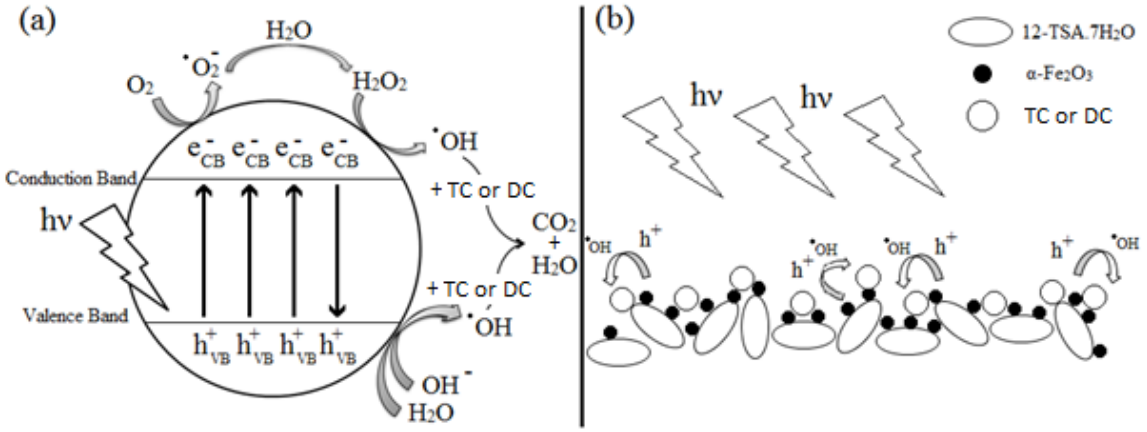

Figure 12. General mechanism of the photocatalysis (a) and photocatalytic activity of α-Fe_2O_3/12-TSA.7H_2O (b).

Kinetics of photocatalytic degradation of pollutants

Figures 13 and 14 displays the plot of $\ln(C_0/C)$ versus reaction time for TC and DC, respectively. The linearity of the plots suggests that the photodegradation reactions approximately follows the pseudo-first order kinetic with a rate coefficient k=0.017 min^{-1} and 0.0074 min^{-1} for TC and DC, respectively. So that, kinetic equations are as below:

(13) R_{TC}=0.017 [TC]

(14) R_{DC}=0.0074 [DC]

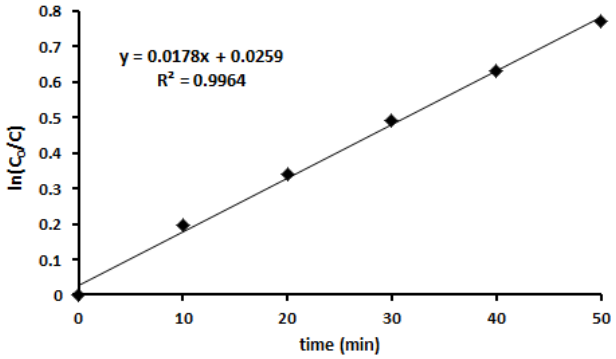

Figure 13. Plot of reciprocal of pseudo-first order rate constant against pH=8, Initial concentration of TC=30 ppm, catalyst concentration=150 ppm, H_2O_2 concentration=0.1 ppm.

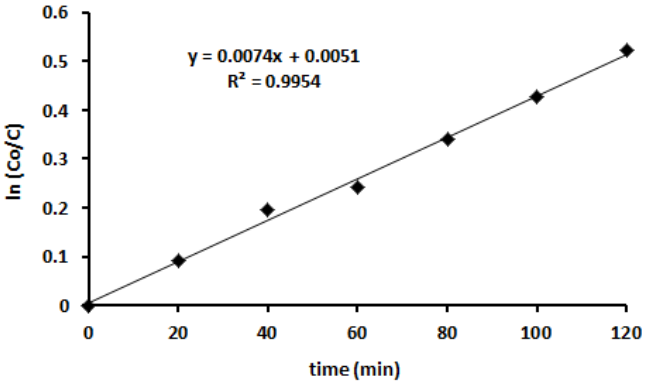

Figure14. Plot of reciprocal of pseudo-first order rate constant against pH=4, Initial concentration of DC=80 ppm, catalyst concentration=150 ppm, H_2O_2 concentration=2 ppm.

The statistical analysis

Analysis of variance (ANOVA) is a set consists of a number of statistical methods used to analyze the differences among group means and their associated procedures. ANOVA was used for graphical analyses of the data to obtain the interaction between the process variables and the responses. The effect on the response was increased by increasing the value of F parameter and decreasing P parameter. The quality of the fit polynomial model was expressed by the coefficient of determination (R^2), and its statistical significance was checked by the Fisher's F-test in the same program. Model terms were evaluated by the P-value. The estimated effects and coefficients of TC and DC degradation processes have been listed in Tables 5 and 6, respectively. In these tables, standard deviation (S), correlation coefficient, pred R-squared and adjusted R-squared values were also reported. The R^2 value is always between 0 and 1. The closer the R^2 value to 1, the stronger the model is and the better the model predicts the response (x%). R^2 values were reported to be 0.9994 and 0.9954 for TC and DC processes, respectively. Due to Table 5 and the significant variables effects on the

response, affect magnitudes of the initial concentration of TC, pH, H_2O_2 concentration and catalyst concentration equal to 32.51, 2.19, 3.32 and 7.22, respectively. Thus, the significant reaction parameters were (the most to the least significant): initial concentration of TC > catalyst concentration > H_2O_2 concentration > pH. Of course, it is necessary to note that despite other three variables, the variable of the initial concentration of TC has a negative effect on the response (–32.51). This means that increasing the initial concentration of TC leads to decrease x% and conversely. In this way, the effects about the variables interaction were reported in Table 5. As can be seen from these results, it is the only interaction of variables, namely pH and the catalyst concentration which have positive effects (1.57). The interaction of the initial concentration of TC with pH, pH with catalyst concentration and H_2O_2 concentration with catalyst concentration have both negative and roughly the same effects on the x% value (–4.23, –1.33 and –3.39, respectively). In Table 5, the coefficients of each term have been reported which are the same term coefficients in response function which they will be given in the following. It is vital to note that P values have been assessed considering Alpha=α=0.05. Table 6 (that is related to the process of DC degradation) shows that initial concentration of DC variable has the highest effect on the response (–6.974). The variables of initial concentration of DC and pH have negative effects and variables of H_2O_2 concentration and catalyst concentration have positive effects on the response. Also, it is seen that the effect of interaction among pH and catalyst concentration is negative (–6.221), while it has the highest effect on the response among other 2-way interactions. In Table 7, complementary results have been listed which have been used for drawing residual plots. Residual values were calculated from subtracting experimental x% values and fitted values.

Table 5. Estimated effects and coefficients for TC degradation process

Term	Effect	Coef	SE Coef	T (Coef/SE Coef)	F value	P value	Result
Constant	-	61.36	0.1711	358.59	-	<0.0001	Significant
Initial Con. of TC	–32.51	–16.25	0.1711	–95.00	9025.02	<0.0001	Significant
pH	2.19	1.09	0.1711	6.40	40.91	0.001	Significant
H_2O_2 Con.	3.32	1.66	0.1711	9.70	94.06	<0.0001	Significant
Catalyst Con.	7.22	3.61	0.1711	21.11	445.62	<0.0001	Significant
Initial Con. of TC×pH	–4.23	–2.12	0.1711	–12.36	152.87	<0.0001	Significant
pH×H_2O_2 Con.	–1.33	–0.67	0.1711	–3.90	15.19	0.008	
pH×Catalyst Con.	1.57	0.78	0.1711	4.58	20.95	0.004	
H_2O_2 Con.×Catalyst Con.	–3.39	–1.70	0.1711	–9.92	98.36	<0.0001	Significant
Center point	-	–2.13	–1.26	–2.92	-	0.027	

S=0.6844, R^2=99.94%, Pred R^2=99.11%, Adj R^2=99.82%

Table 6. Estimated effects and coefficients for DC degradation process

Term	Effect	Coef	SE Coef	T (Coef/SE Coef)	F value	P value	Result
Constant	-	73.608	0.128	575.55	-	<0.0001	Significant
Initial Con. of DC	–6.974	–3.487	0.139	–25.02	625.97	<0.0001	Significant
pH	–3.739	–1.869	0.139	–13.41	179.92	<0.0001	Significant
H_2O_2 Con.	2.596	1.298	0.139	9.31	86.76	<0.0001	Significant
Catalyst Con.	4.341	2.171	0.139	15.57	242.58	<0.0001	Significant
pH×Initial Con. of DC	2.949	1.474	0.139	10.58	111.92	<0.0001	Significant
pH×Catalyst Con.	–6.221	–3.111	0.139	–22.32	498.17	<0.0001	Significant
pH×H_2O_2 Con.	0.959	0.479	0.139	3.44	11.83	0.007	
Initial Con. of DC×H_2O_2Con.	2.659	1.329	0.139	9.54	90.99	<0.0001	Significant
Catalyst Con. ×H_2O_2Con.	2.884	1.442	0.139	10.35	107.04	<0.0001	Significant
Center point	-	–1.67	1.116	–0.722	-	0.034	

S=0.557465, R^2=99.54%, Pred R^2=97.11%, Adj R^2=99.08%

Table 7. Residual values

Exp. No.	For TC process			For DC process		
	x%	Fit	Residual (x%–Fit)	x%	Fit	Residual (x%–Fit)
1	66.32	66.7703	-0.4503	78.19	76.79082	1.399178
2	85.95	85.3212	0.6288	74.65	81.47457	-6.82457
3	73.29	73.4112	-0.1212	84.62	83.37207	1.247928
4	53.22	53.0988	0.1212	72.66	71.80082	0.859178
5	45.07	44.4022	0.6678	64.93	71.01082	-6.08082
6	60.38	60.1000	0.2800	74.08	74.54895	-0.46895
7	88.44	89.1078	-0.6678	83.09	78.77957	4.310428
8	43.64	44.1281	-0.4881	66.15	68.91957	-2.76957
9	74.61	74.5137	0.0963	72.99	72.19832	0.791678
10	47.92	48.5488	-0.6288	73.67	73.70582	-0.03582
11	38.91	38.4597	0.4503	65.17	68.51707	-3.34707
12	74.28	74.3372	-0.0572	74.66	72.60082	2.059178
13	37.71	37.8063	-0.0963	69.22	67.72707	1.492928
14	48.72	48.8022	-0.0822	80.09	74.49582	5.594178
15	45.62	45.5628	0.0572	73.09	68.12957	4.960428
16	59.79	60.1000	-0.3100	74.44	74.54895	-0.10895
17	77.13	77.0478	0.0822	87.67	86.06707	1.602928
18	60.13	60.1000	0.0300	73.78	74.54895	-0.76895
19	80.86	80.3718	0.4882	73.28	77.19332	-3.91332

Figure 15 shows the graphical results of TC degradation process. In order to compare the variables effect (from the viewpoint of magnitude) on the response, the Figure 15a could be investigated which is one Pareto chart of the standardized effects. In this Figure, those variables whose effects on response is negative (–) or positive (+) have been marked. The results revealed that the effect of the initial concentration of TC on the x% is greater than other variables effect (at least four times) but the effect of this variable is negative i.e. increasing or decreasing the

initial concentration of TC leads to decrease and increase x%, respectively. In order to better investigate the residual values, residual plot versus Exp. No. has been illustrated in Figure 15b. As it is seen, nine points (residuals) are located under zero line (negative) and ten points above zero line (positive). Due to this and comparing distance of points from zero line, it could be said that residual distribution is normal. An extremely useful procedure is to construct a normal probability plot of the residuals. If the underlying error distribution is normal, this plot will resemble a straight line. Figure 15c shows normal probability plot. In this plot, it is fully clear that residuals distribution is normal because points (especially central points) are close to straight line. If the model is correct and if the assumptions are satisfied, the residuals should be structure less; in particular, they should be unrelated to any other variable including the predicted response. A simple check is to plot the residuals versus the fitted values. Figure 15d displays plot of residuals versus fitted values. Graphical results of DC degradation process have been illustrated in Figure 16. Pareto chart in Figure 16a shows that greatest and smallest effect on the response were respectively related to initial concentration of DC and interaction among pH and H_2O_2 concentration variables. The uniform distribution of points above and below the zero line in Figure 16b shows that residuals in experiments of DC degradation process are normally distributed. Also, normal probability plot of the process has been illustrated in Figure 16c which proximity of points to the line and centralization of points indicate the normality of residuals. Mathematical models representing TC and DC photocatalytic degradation in the range studied can be expressed by the following equations, respectively:

Response = x% (TC) = 61.36 – 16.25 A + 1.09 B + 1.66 C + 3.61 D – 4.23 AB – 1.33 BC + 1.57 BD – 3.39 CD + 3.97 ABC – 4.00 ABD + 1.59 BCD ± . . .

Response = x% (DC) = 73.608 – 3.487 A – 1.869 B + 1.298 C + 2.171 D + 1.474 BA – 3.111 BD + 0.479 BC + 1.329 AC + 1.442 DC ± . . .

Where A, B, C and D are the initial concentration of pollutant, pH, H_2O_2 concentration and catalyst concentration, respectively.

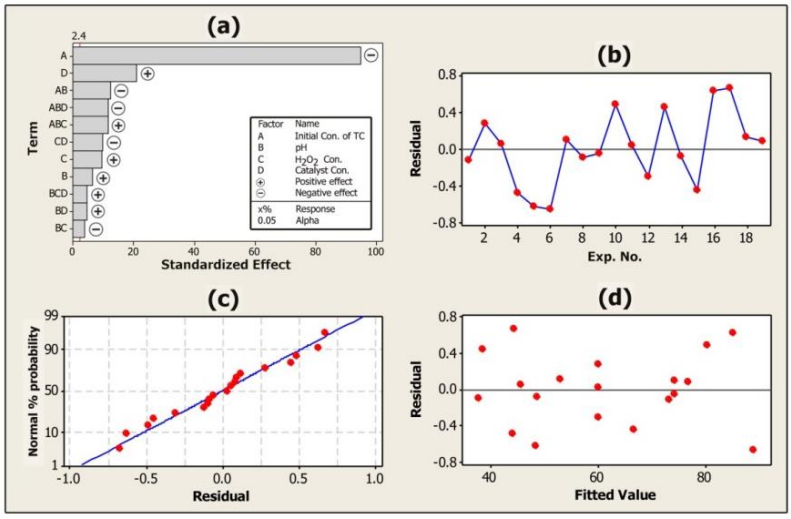

Figure 15. (a) Pareto chart of the standardized effects, (b) plot of residuals versus Exp. No., (c) Normal probability plot and (d) plot of residuals versus fitted values related to TC degradation process.

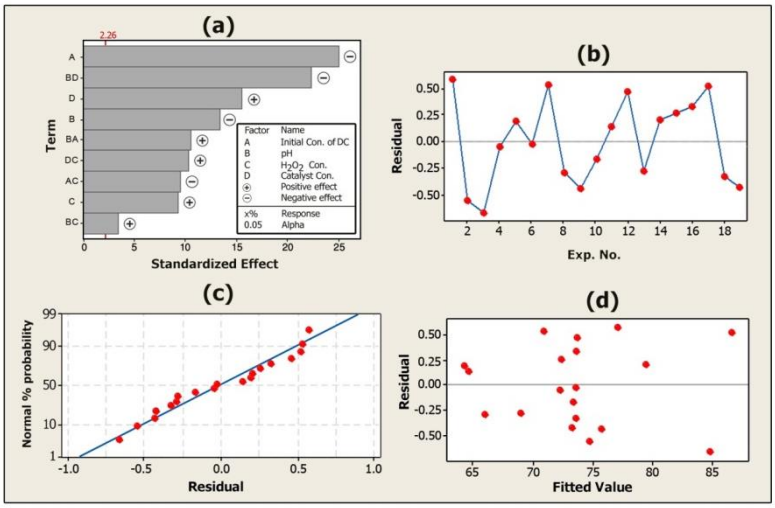

Figure 16. (a) Pareto chart of the standardized effects, (b) plot of residuals versus Exp. No., (c) Normal probability plot and (d) plot of residuals versus fitted values related to DC degradation process.

In Figure 17, the plots of main effects related to TC degradation process have been shown. These plots indicate that of four main effects, only the variable of the initial concentration of TC has a negative effect on response; effects of other variables on response were positive. In effect, increasing the initial concentration of TC and decreasing pH, H_2O_2 concentration and catalyst concentration will be caused to decrease and increase x%, respectively (if the interaction effect of variable is ignored). The slope of line in main effect plots is one indicator of magnitude related to the variable effect on the response. Therefore, the order of affecting variables from magnitude viewpoint is as initial concentration of TC > catalyst concentration > H_2O_2 concentration > pH which confirm the results of Figure 15a. The plots of main effects (related to the process of DC degradation) have been illustrated in Figure 18. These plots show that as the level of initial concentration of DC and pH variables increase, then the response decreases and as the level of H_2O_2 concentration and catalyst concentration variables increase, then the response increases. Also, because the plots of initial concentration of DC and H_2O_2 concentration variables have highest and lowest slope respectively, then they have greatest and smallest effects on the response, respectively.

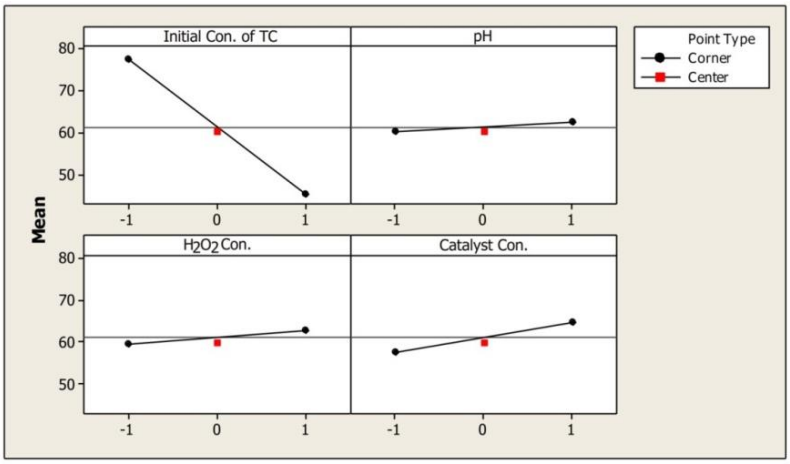

Figure 17. Main effects plot for TC degradation process.

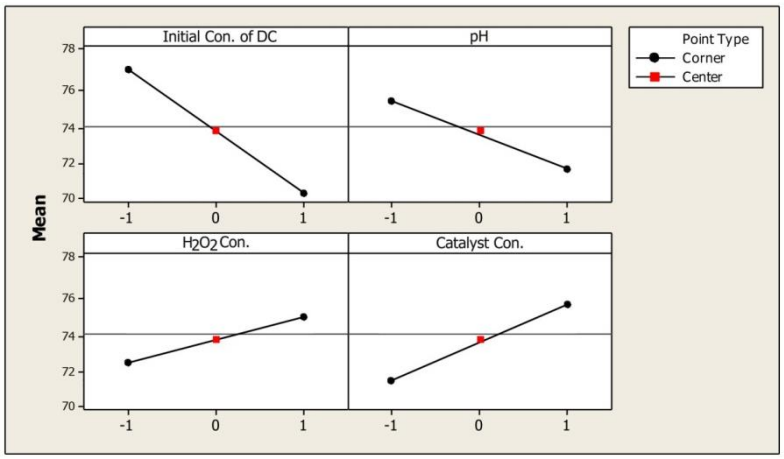

Figure 18. Main effects plot for DC degradation process.

In Figure 19, interaction plots for TC degradation process have been presented. Generally, in such plots the more parallel the lines, the lower the interaction effect would be and the more intersecting the lines, the higher the interaction effect would be. As it is observed, there is a significant interaction effect among pH and H_2O_2 concentration, pH and catalyst concentration, H_2O_2 concentration and catalyst concentration variables. Generally, considering the interaction effects is very important because it may place the unpredictable effects on the response. For example, based on the results of Figure 15a even though H_2O_2 concentration had simply a positive effect on x%, the maximum x% was achieved in those conditions where H_2O_2 concentration was at its minimum level (see Exp. No 7 in Table 4). For the same reason, the interaction effect of variables should not be ignored in studying variables for reaching optimal conditions. In Figure 20, Interaction plots of DC degradation process have been shown. It is seen that there is significant interaction between pH and catalyst concentration variables. This interaction among pH and initial concentration of DC variables and also between catalyst concentration and H_2O_2 concentration are rather found.

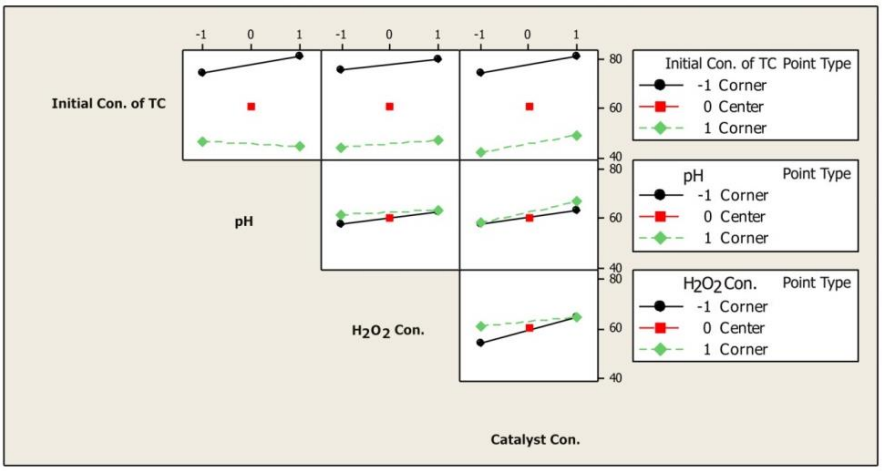

Figure 19. Interaction plot for TC degradation process.

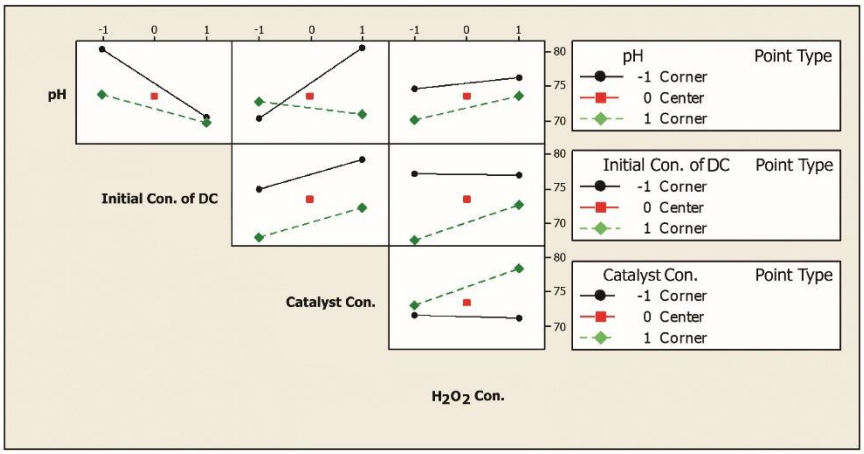

Figure 20. Interaction plot for DC degradation process.

Conclusions

The results revealed that:

1. Spherical α-Fe_2O_3 NPs had been successfully synthesized and supported on the surface of 12-TSA.7H_2O through FHRC method with no decrease of NPs photocatalytic efficiency and chemical change of 12-TSA.7H_2O which are indicative of being effective this supporting method.
2. While supporting α-Fe_2O_3 NPs on the surface of 12-TSA.7H_2O help to recover them from the medium and reusing them, it causes to enhance their photocatalytic activities.
3. Photocatalytic effect of α-Fe_2O_3/12-TSA.7H_2O on the TC and DC degradation is greater than pure α-Fe_2O_3 NPs.
4. The statistical analysis results indicated that the model used in this paper is significantly reliable and valid.
5. In the processes of the TC and DC photocatalytic degradation using α-Fe_2O_3/12-TSA.7H_2O, four parameters of pH, the initial concentration of pollutant, catalyst concentration and H_2O_2 concentration are effective on x%.
6. The interaction effects of variables are very important and should be considered for optimizing the conditions because it significantly affects the x%.
7. The optimum conditions for the TC degradation process by α-Fe_2O_3/12-TSA.7H_2O is as pH=8, initial concentration of TC=150 ppm, catalyst concentration =150 ppm and H_2O_2 concentration=0.1 ppm so that they cause to reach maximum degradation (88.44%).
8. The optimum conditions for the DC degradation process is as pH=4, initial concentration of DC=80 ppm, catalyst concentration =150 ppm and H_2O_2 concentration=2 ppm so that they cause to reach maximum degradation (87.67%).
9. The kinetics of TC and DC photocatalytic degradation reactions are of the pseudo-first order with k=0.0178 and 0.0074 min^{-1}, respectively.

Acknowledgments: This work was financially supported by Islamic Azad University of Arak, Iran.

References

[1] Novo. A, Andre. S, Viana. P, Nunes. O. C, Manaia. C. M, Water. Res, 2013, 47, 1875.
[2] Kummerer. K, Chemosphere, 2013, 75, 417.
[3] Brown. K. D, Kulis. J, Thomson. B, Chapman. T. H, Mawhinney. D. B, Sci. Total Environ. 2066, 366, 772.
[4] Pailler. J. Y, Krein. A, Pfister. L, Hoffmann. L, Guignard. C, Sci. Total Environ. 2009, 407, 4736.
[5] Hou. J, Wang. C, Mao. D, Luo. Y, Environ. Sci. Pollut. Res. Int. 2016, 23, 1722.
[6] Pourmoslemi. S, Mohammadi. A, Kobarfard. F, Amini. A, Water Sci. Technol. 2016, 74, 1658.
[7] Neatu. S, Macia-Agullo. J. A, Concepcion. P, Garcia. H. J, Am. Chem. Soc. 2014, 136, 15969.
[8] Chen. M, Liu. J, Chao. D, Wang. J, Yin. J, Lin. J, Fan. H. J, Shen. Z. X, Nano Energy, 2014, 9, 364.
[9] Rancourt. D. G, Julian. S. R, Daniels. J. M. J, Magn. Mater. 1985, 49, 305.
[10] Hill. C. L, Chem. Rev. 1998, 98, 1.
[11] Pope. M. T, Heteropoly and Isopoly Oxometalates, SpringerVerlag, Berlin, 1983.
[12] Kozhevnikov. I. V, Chem. Rev. 1998, 98, 171.
[13] Es'haghi. Z, Hooshmand. S. J, Sep. Sci. 2015, 38, 1610.

[14] Wang. L. Zhou. B, Liu. J, Prog. Chem. 2013, 25, 1131.
[15] Judd. D. A, Netlles. H. J, Nevis. N, Snyder. J. P, Liotta. D. C, Tang. J, Ermolieff. J. J, Schinazi. F. R, Hill. C. L. J, Am. Chem. Soc. 2001, 123, 886.
[16] Wang. X, Liu. J, Li. J, Liu. J, Inorg. Chem. Commun. 2001, 4, 372.
[17] Lin. Z, Zhongqun. L, Wenjun. C, Shaojin. C, Radioanal. J. Nucl. Chem. 1996, 205, 49.
[18] Heylen. S, Smeekens. S, Kirschhock. C. E. A, Parac-Vogt. T. N, Martens. J. A, Energy Environ. Sci. 2010, 3, 910.
[19] Lihua. B, Qizhuang. H, Qiong. J, Enbo. W. J, Mol. Struct. 2001, 597, 83.
[20] Xia. Y, Xiong. Y, Lim. B, Skrabalak Angew. S. E, Chem. Int. Ed. 2009, 48, 60.
[21] Zhang. S, Fan. Q, Gao. H, Huang. Y, Liu. X, Li. J, Xu. X, Wang. X. J, Mater. Chem. A. 2016, 4, 1414.
[22] Zhang. S. Li. J, Wang. X, Huang. Y, Zeng. M, Xu. J. J, Mater. Chem. A. 2015, 3, 10119.
[23] Jun. Y. W, Choi. J. S, Cheon. J.J, Chem. Commun. 2007, 12, 1203.
[24] Chen. J, Xu. L, Li. W, Gou. X, Adv. Mater. 2005, 17, 582.
[25] Raming. T. P, Winnubst. A. J. A, Van Kats. C. M, Philipse. A. P. J, Colloid Interface. Sci. 2002, 249, 346.
[26] Walter. D, Thermochim. Acta 2006, 445, 195.
[27] Shekhah. O, Ranke. W, Schule. A, Kolios. G, Schlogl. R, Angew. Chem. Int. Ed. 2003, 42, 5760.
[28] Mishra. M, Chun. D. M, Appl. Catal. A 2015, 498, 126.
[29] Farahmandjou. M, Soflaee. F, Phys Chem. Res. 2015, 3, 191.
[30] Liang. H, Liu. K, Ni. Y, Mater. Lett. 2015, 159, 218.
[31] Diab. M, Mokari. T, Inorg. Chem. 2014, 53, 2304.
[32] Jiang. T, Poyraz. A. S, Iyer. A, Zhang. Y, Luo. Z, Zhong. W, Miao. R, El-Sawy. A. M, Guild. C. J, Sun. Y, Kriz. D. A, Suib. S. L. J, Phys. Chem. 2015, 119, 10454.
[33] Askarinejad. A, Bagherzadeh. M, Morsali. A. J, Exp. Nanosci. 2011, 6, 217.
[34] Tadic. M, Panjan. M, Damnjanovic. V, Milosevic. I, Appl. Surf. Sci. 2014, 320, 183.
[35] Bharathi. S, Nataraj. D, Mangalaraj. D, Masuda. Y, Senthil. K, Yong. K. J, Phys. D, Appl. Phys. 2010, 43, 1.
[36] Nabizadeh. R, Jahangiri Rad. R, Res. J. Nanosci. Nanotechnol, 2016, 6, 1.
[37] North. E. O, Bailar. J. C, Jonelis. F. G, Inorg. Synth. 2007, 1, 129.
[38] Bamoharram. F. F, Molecules 2009, 14, 3214.
[39] Kozhevnikov. I. V, Sinnema. A, Jansen. R. J. J, Bekkum. H. V, Catal. Lett. 1994, 27, 187.
[40] Enzo. S, Polizzi. S, Benedetti. A, Zeitschrift für Kristallographie 1985, 170, 275.
[41] Yao. K, Basnet. P, Sessions. H, Larsen. G. K, Hunyadi Murph. S. E, Zhao. Y, Catal. Today 2016, 270, 51.
[42] Guo. S, Zhang. G, RSC Adv. 2016, 6, 2537.